An overview of the TIMAX experiment

Flavio D'Amico, João Braga, Thyrso Villela, Alexandre M. R. Alves
Edson R. Silva and José A. C. F. Neri
Divisão de Astrofísica Instituto Nacional de Pesquisas Espaciais-INPE
CP 515, S. J. dos Campos, SP, 12201-970, Brazil

Recebido em 7 de março, 1995

Neste artigo descrevemos o experimento TIMAX, o primeiro telescópio imageador de raios-X totalmente concebido, construído e lançado por um país do Hemisfério Sul. A capacidade de imageamento é obtida através do uso de uma máscara baseada num padrão URA 7 x 5. Mostra-se uma maneira de se obter uma antimáscara a partir da máscara original, com o uso de padrões URA, sem a adição de peso extra à experiência e sem manipulações mecânicas complicadas. O experimento TIMAX tem uma resolução angular de 1°,7 num campo de visada de 10° x 10° (FWHM). O plano de detectores sensíveis à posição consiste em 35 cintiladores cilíndricos de NaI(Tl), operando na faixa de 30-100 keV, com uma área geométrica total de $\sim$ 400 cm^2. São apresentadas imagens obtidas durante a calibração do instrumento, mostrando as vantagens da utilização de uma antimáscara para a obtenção de imagens. Utilizando-se o ruído de fundo medido no primeiro vôo em balão estratosférico do experimento, mostra-se que a sensibilidade é de $\sim$ 1.2 x 10^{-4} fótons cm^{-2} s^{-1} keV^{-1} na banda de 60-70 keV, para um tempo de integração de 8 horas para uma atmosfera residual 2 g cm^{-2}. Esta sensibilidade permite a detecção da maioria das fontes na região do Centro Galáctico.

The TIMAX experiment, the first X-ray imaging telescope entirely conceived, built and launched by a country in the Southern Hemisphere, is described. The imaging capabiblity is provided by an extended mask based in a 7 x 5 URA pattern. A new and elegant technique for providing an "antimask" on URA coded-mask systems, without the addition of either extra weight or complex mechanical maneuvering systems to the experiment, is introduced. The TIMAX experiment has a.n angular resolution of 1°.7 in a 10° x 10° FOV(FWHM). The position-sensitive detector plane consists in 35 cylindrical NaI(Tl) scintillators, operating in the 30 - 100 keV energy range, with a total area of $\sim$400 cm^2. Images produced during the calibration of the instrument in the laboratory are presented, showing the advantages of the mask-antimask imaging technique. The background measured at balloon altitudes on the first flight of the experiment demonstrates that the sensitivity of the telescope is $\sim$ 1.2 x 10^{-4} photons cm^{-2} s^{-1} keV^{-1} in the 60-70 keV range, for an integration time of 8 hours at a residual atmosphere of 2 g cm^{-2}. This sensitivity allows the detection of most X-ray sources in the Galactic Center region.

I. Introduction

In the hard X-ray domain of the eletromagnetic spectrum ($\sim$ 10 to 200 keV) the focalization of photons is not yet feasible with current technology. In the soft X-ray range, the *grazing incidence* focussing technique can be used, and a large number of images of celestial sources has been produced by several experiments, including the EINSTEIN[1], EXOSAT[2], ROSAT[3], and, more recently, ASCA[4] satellites. Nevertheless, this technique is limited to energies $\leq$ 10 keV (this is the upper limit energy for the Japanese ASCA satellite). The lack of imaging power has been one of the greatest difficulties in the study of hard X-ray and soft gamma-ray emission by a variety of interesting objects in the universe. The detection of non-thermal radiation coming from accreting matter in the vicinity of neutron stars or black holes in binary systems, as well as the study of high-energy radiation coming from supernova remnants and extragalactic sources like galaxy clusters and active galactic nuclei, are crucial for the building of thorough, complete models for a variety of hard X-ray sources in the universe. Imaging is essential for the unambiguous spectral study of these sources. As an example we may consider the well-known 511 keV line emission originated in the general direction of the center of our Galaxy: is this emission being produced by a single object? Is the source diffuse? What is the actual spatial distribution of the emission source and how does the spectrum vary as a function of position? Clearly, imaging power with good angular resolution is of great importance in the quest to answer such questions.

The coded-aperture imaging approach in the hard X-ray range was first addressed in 1968 by Dicke[5]. His proposal consisted in a spatial modulation of the incoming radiation by means of a pattern of apertures in an otherwise opaque "mask" in a position sensitive detector tector (PSD) placed under the mask. In this technique, each photon is treated individually, and if we could record the position (x, y) of interaction of a photon in the PSD and measure its energy, whith a large number of photons detected, we have an image, that is, a spatial distribution of intensities in a field of view (FOV), if one uses a suitable mask aperture pattern. Although a large number of patterns has been successfully used, one of the best solutions is the URA (Uniformly Redundant Arrays), defined by Fenimore and Cannon[6] in 1978. These arrays allow "perfect imaging" (no side lobes) and high signal-to-noise ratios. For a detailed description of URA properties and image reconstruction techniques, see [7] and references therein.

In the next section the main scientific objectives of the TIMAX experiment are reviewed. In the following sections we will examine some important characteristics of the TIMAX project, with emphasis on the original mechanical method of providing an antimask of the original mask, which is the principal contribution of the experiment for future imaging telescopes. The calibration of the imaging system and the results of the first balloon flight of the experiment are also described.

2. Scientific objectives

Our main scientific goal with the TIMAX experiment is the study of the Galactic Center (GC) region, a rich Southern Hemisphere field of highly variable X- and γ-ray sources. Due to observations carried out by coded-aperture imaging telescopes such as SL2-XRT[8], GRIP[9], TTM[10], ART-P[11] and SIGMA[12], our knowledge about the X-ray sources on the GC region has increased significantly over the last few years. ARTP and SIGMA have played a special role: their angular resolution, sensitivity and broad-band energy range, when observations of the two telescopes are combined, were responsible for both a detailed knowledge of the source spatial distribution and the discovery of several new hard X-ray sources in the vicinity of the GC.

Using the Caltech GRIP experiment, Cook et al.[13] found that the bulk of the GC hard X-ray/soft γ-ray emission was coming from the previously unremarkable Einstein source 1E1740.7-2942[14] located $0°.8$ away from the dynamical center of the Galaxy in Sgr A^*. The SIGMA coded-aperture imager onboard the GRANAT satellite measured a strong feature in the spectrum of this object[15], readily interpreted as intense 511keV annihilation radiation. The line was centered at ~480keV and was extremely broad (~240keV FWHM), with a total flux of $\sim 1.3 \times 10^{-2}$ photons cm^{-2} s^{-1}, which is one order of magnitude stronger than the typical mean flux measured during the 1970's. This fact caused great excitement in the γ-ray astronomy community, inasmuch as the origin of the 511 keV line had been one of the main puzzles in this field since its discovery and subsequent detections in the 1970's (see [16] and references therein). After the SIGMA discovery, evidence of an annihilation line was also found in the spectra of other galactic sources, including the X-ray nova in Musca[17].

In 1990, the SIGMA experiment discovered another hard X-ray source near the GC, GRS 1758-258[18,19]. This source is 40 arcmin away from the bright quasiperiodic source GX5-1; probably much of the hard X-ray emission attributed to this object in the past was in fact coming from GRS 1758-258. Further observations of the GC region have shown that most of the sources are variable in nature. Another set of images produced by SIGMA between February 17 and March 12, 1992[18], showed the presence of five bright sources in the 40-100keV range: 1E1740.7-2942; the X-ray burster GX354-0 (with a flux at a level of about 75mCrab and increasing gradually); the well-known X-ray pulsar GX1+4 (at an average level of 35 mCrab, apparently variable); the globular cluster Terzan 2 (about 20 mCrab average flux); and the Spacelab-2 source SLX 1735-269 (also ~20 mCrab average flux) which had been discovered at softer energies[20] with a coded mask X-ray telescope. GX1+4 (which was detected in 1982 at energies above ~200keV[21]) has also been recently detected in a very intense outburst state by the BATSE experiment onboard the Compton Gamma Ray Observatory (CGRO) with a pulse period of 120.567± 0.005 s, showing that it is currently undergoing another spin-down phase[22].

All these exciting discoveries and observations show clearly that the nature and spatial distribution of the GC sources are still far from being determined with accuracy. Imaging telescopes, which can measure both locations and spectra of the sources, subtracting background simultaneously, are very important to the further study of this region.

3. Instrument description

3.1 The Mask

The mask of the TIMAX experiment is showed in the Figure (1). It consists in a 2 x 2 cyclic repetition of a basic 7 x 5 URA pattern, except for one row and one column at the edges, attached in one of the sides of a carbon fiber wheel (completely transparent for hard X-rays). Each opaque element is a 4.45cm-side square made of 3mm-thick lead and 1mm-thick copper material providing a graded shield. In the opposite side of the wheel, a bar which is also part of the mask and is made with the same materials as the individual elements, is supported in such a way that it is free to rotate around the center of the mask. As can be seen in Figure 1, if the bar rotates by 90° and the mask by 180° we obtain an antimask of the original mask with the exception of the central element, which always remains opaque. This is a new and elegant way to get an antimask in coded-aperture telescopes with neither addition of an extra weight to the experiment nor further mechanical complex manipulations, which have always hindered the operation of similar experiments. This method can be applied to any URA dimensions, not only the 7 x 5 one. As it will be seen in the next section, the primary objective of the mask/antimask imaging technique is to suppress systematic noise in the detector plane by means of a subtraction of two counts distributions obtained with equal integration time and with the antimask. In this way the systematic noise is subtracted out and the only remaining sources of noise are differences in sensitivity across the PSD and Poissonian statistical noise. For a detailed discussion about image reconstruction using masks and antimasks, see [23].

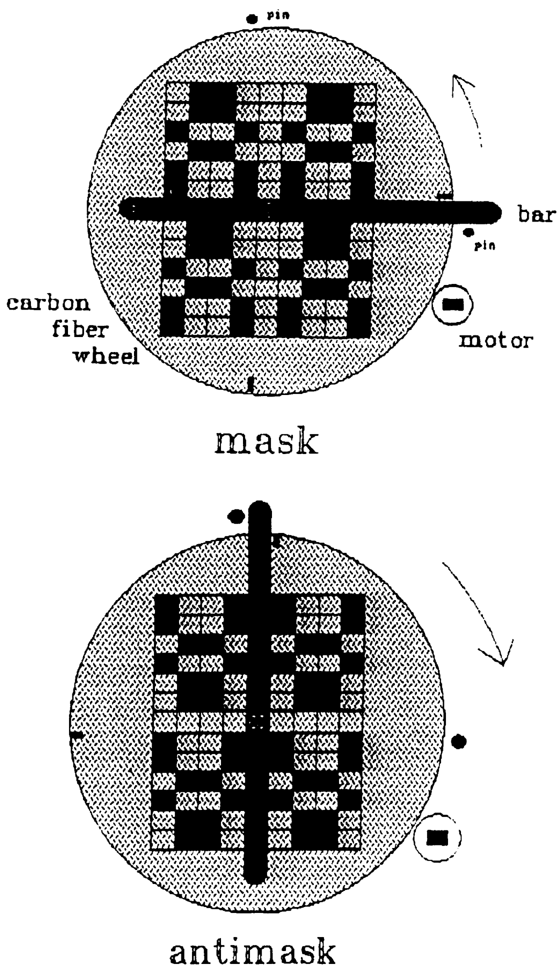

Figure 1: The mask (and antimask) of the TIMAX experiment.

3.2 Detectors

The position-sensitive detector (PSD) plane of TIMAX consists of 35 cilindrical NaI(Tl) detectors, 2-mm thick and 4.45 cm in diameter, with an useful sensitive diameter of 3.18 cm, placed in a matrix array of 7 x 5 to be compatible with the URA pattern used, and defining (due to detector-mask distance and basic mask element dimensions) a sky element of ~ 1°.7. The total geometric area is ~ 400 cm^2. Each detector is coupled to a photomultiplier. The 35 photomultipliers are powered by five high voltage units that operate in a nominal voltage of ~ 900 V. The detectors operate in the 30-100 keV range, set by lower-level (ULD) and upper-level (ULD) discriminators. The lower limit is set due the low atmospheric transmition below 30 keV and the upper limit is due to low absortion efficiency of the 2mm-thick crystal scintillator above 100 keV.

3.3 Angular Resolution and Field of View

In a coded mask telescope, the geometrical angular resolution is obtained from:

$$R = \frac{d}{D} \, , \tag{1}$$

where d is the size of each cell in the mask (4.45 cm for TIMAX) and D the distance between the mask an the PSD. An obvious way of improving the angular resolution is to increase the mask-PSD separation. Due to weight and mechanical restrictions on the payload, we have used a distance of $D = 150$ cm and got a resolution of $\sim 1^{\circ}.7$. A collimator made of 1mm-thick copper pipes coated with 0.5mm lead sheets was placed in front of the detector system in order to define a field-of-view of $10^{\circ} \times 10^{\circ}$ full width at half maximum (FWHM), which is totally coded by the mask. The whole detector system is passively shielded on the sides and on the back by 3mm-thick copper and 1-mm lead plates.

3.4 Electronics

Each PMT pulse produced by a scintillation event due to a X-ray interaction in one of the detectors is height-analized in 32 equally-spaced energy channels. The on-board electronics then identifies the detector in which the event ocurred and builds a digital word of 11 bits with these information (5 bits witll energy information and 6 bits with position information). The event time (1 ms resolution) read from an internal clock is then added to the frame. A microprocessor formats all the information, including housekeeping data (temperature, atmospheric pressure, ...) of the gondola, for subsequent transmission by telemetry. There is no data storage on-board.

3.5 Balloon gondola

A photograph of the gondola used by TIMAX is shown in Figure 2. In order to allow the telescope to point at high elevation angles, the telescope support system was designed to be placed off-center in the balloon gondola. In this way, the detector system, including the collimator and shielding parts, and the coded-mask which is attached to a carbon-fiber wheel driven by a motor, were placed in one side of the gondola in a "tower-like" metal structural frame supported and balanced by a horizontal axis that allows the telescope to point in a specific elevation angle. On the other side were allocated the electronics rack, the telemetry system and the batteries. The entire gondola rotates in azimuth, with the pointing in a specific azimuth angle being controlled and stabilized by a system based on a geomagnetic sensor with a accuracy of $\sim 1^{\circ}$. The telescope "tower" is positioned in elevation by a shaft encoder with a $\sim 0.5^{\circ}$ accuracy. The pointing system can be operated in manual mode through commands sent from the ground or in a semi-automatic way that follows the source path in the sky, given its initial position and the balloon velocity vector. The total weight of the experiment (including gondola frame, telescope, electronics and telemetry racks, magnetometer, batteries and ballast system) is ~600 kg.

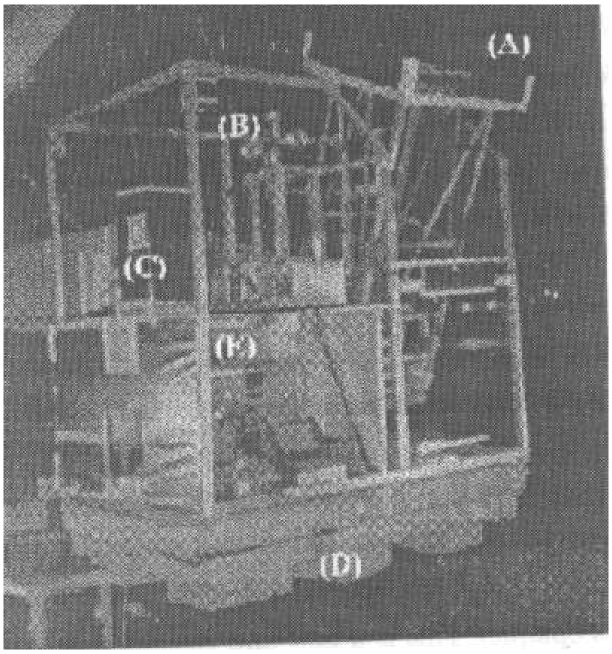

Figure 2: The Gondola of the TIMAX experiment, in a photo taken some minutes before launch. Some of the main parts are: (A) "tower" that houses the telescope; (B) the azimuth positioning system; (C) magnetometer, to feed the azimuth positioning system; (D) on-board electronics and telemetry racks; (E) the shock absortion system.

4. Laboratory images

The first laboratory images produced by the TIMAX experiment are discussed in detail in [24]. Here we discuss the flat-fielding technique employed and show the results obtained in the laboratory.

One of the important stages in the development of coded-mask telescopes is to calibrate the performance of the imaging system in the laboratory. In this stage, all the components are in flight configuration, with the data acquired by the on-board electronics being transmitted by telemetry.

The mask-antimask technique is suitable to subtract, from the final image, effects due to systematics variations among the different detectors (or throughout a unique detector) in the PSD plane[23], but this isn't the only correction to be applied. One important feature is that the PSD detectors have completely different sensitivities. This means that the number of counts of two distinct detectors are different for non-variable source of X-rays. So we have to correct this effect in the final image. The way to do this is to *flat-field* the image. In a coded-mask telescope the flat-field technique was for the first time applied in the University of New Hampshire balloon-borne Gamma-ray imagin, experiment DGT[25]. The method consists in exposing all the PSD detectors (or detector) **uniformly** to the same known (that means, calibrated) intense (to minimize statistical fluctuations) radioactive source withouth the use of a mask or an antimask. When this is done we assure that the different counts in the PSD detectors (or detector) are uniquely due to intrinsic differences in sensitivity. We can then define correction factors to be applied to each detector (or each portion of a unique detector) in order to flat-field the entire detector plane.

In the TIMAX experiment, however, we flat-field the images in a little different way than that applied in DGT. We corrected *channel by channel* the counts of the 35 detectors using the average value of the counting rates of all 35 detectors. In order to determine the correction factors, we performed a long integration time data acquisition using a strong radioactive source placed far away from the detector plane (so that its distance to all detectors is approximately the same), and with the coded-mask removed so that all detectors were equally illuminated.

Let $k_{(ji)}$ be the number of counts for the j detector in the i channel (for TIMAX i run since 1 to 32). Hence a corrector factor beta is defined as follows

$$\beta_{j,i} = \frac{k_{j,i}}{(1/35)\sum_{j=1}^{35} k_{(j,i)}} \,. \qquad (2)$$

So, for each detector we have 32 β factors and for a given observation, if $c_{(j,i)}$ is the number of counts of channel i on detector j, the flat-fielded number of counts $C_{(j,i)}$ is then given by:

$$C_{(j,i)} = \frac{c_{j,i)}}{\beta_{(j,i)}} \qquad (3)$$

As can be seen the β factor introduces a multiplicative correction in the image.

The images presented here were otained with a 100 mCi^{241}Am source placed at a distance of ~45 m from the mask. Such a distance is sufficient to ensure that no magnification factor would be present in the shadowgram of the mask on the detector plane (so as to simulate an astronomical observation). Each image is displayed as follows: in the x axis we display 7 detectors, resulting in an angular size of $\sim 12°$; in the y axis we display 5 detectors, resulting in an angular size of $8°.5$; in the z axis the recorded counts are displayed. The z-axis is not shown for a better image display.

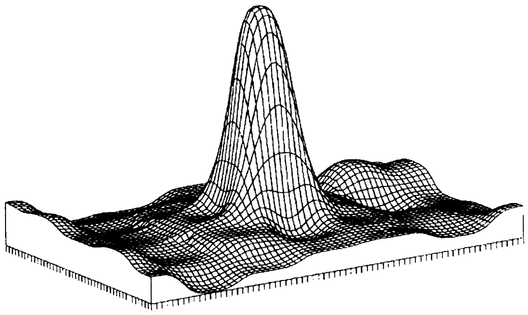

Figure 3: Laboratory Image of the TIMAX experiment. This image was built with the telescope in the mask position (SNR = 18.57). The angular size is $12° \times 8°.5$. For axis information see text above.

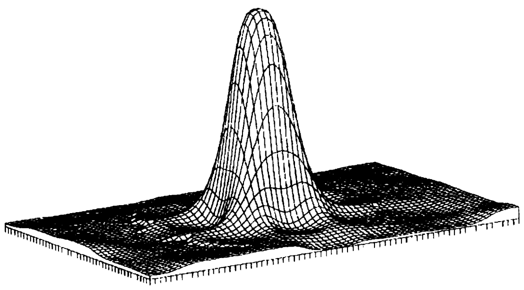

Figure 4: Flat-fielded image obtained with the telescope in the mask position (SNR = 69.30).

Figure 3 displays an image obtained with the telescope in the mask position (see Figure 1), for an integration time of 2 hours.

This image has a signal to noise-ratio[26] of 18.57. We applied to this raw image the multiplicative method of correction, by multiplicating channel by channel the counts in the 35 detectors by the, β-factors described above. The result is presented in the Figure 4, which has a SNR of 69.30. The improvement in SNR is roughly a factor of 4.

In Figure 5 we present an image obtained with the telescope in the antimask position with the same integration time of two hours. The SNR of this image is 15.87 which represents a of degradation factor of ~

1.2 with respect to Figure 3. This loss in SNR, which is explained in detail in [23], is due to the fact that the central element remains always opaque in both the mask and the antimask (see Figure 1), so the antimask is not a perfect URA.

In Figure (6) an image built with the mask-antimask technique is presented. To build this image we integrated for 1 hour with the telescope in the mask configuration and for another hour with the telescope in the antimask configuration. The count distributions were then subtracted. The SNR of this image is 25.47, a factor of improvement of 1.4 or 37% in the SNR with respect of Figure (3). This shows the efficiency of the mask-antimask imaging technique.

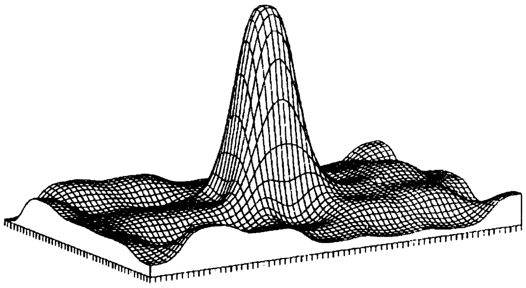

Figure 5: Image built with the telescope in the antimask position (SNR = 15.87).

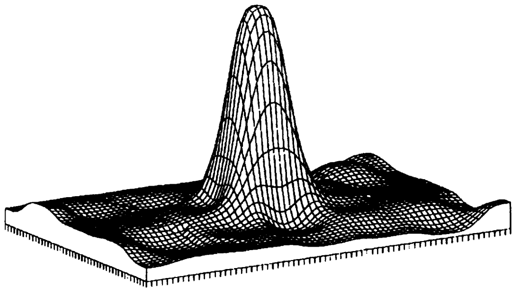

Figure 6: Image built with the mask-antimask technique (SNR = 25.47).

Finally our last image is presented in Figure 7, multiplying the image showed in Figure 6 by the β-factors, that means, by introducing the multiplicative method in an image obtained by the subtractive mask-antimask technique. This final image has a SNR of 140.06. This means an improvement of a factor of 2 when compared with Figure 4. This, undoubtely, shows the efficiency of the subtractive method to remove from the final image artifacts that could be included by systematic variations in the counts among the 35 detectors and the efficiency of the multiplicative method to correct the differences due to different sensibilities among the 35 detectors.

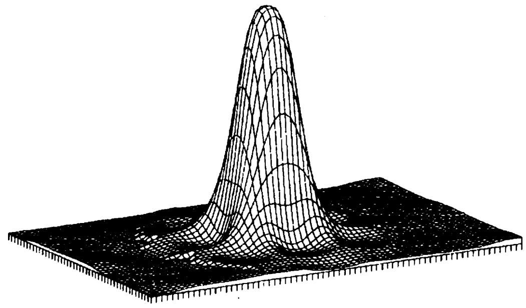

Figure 7: Image obtained with the mask-antimask subtractive technique and the multiplicative correction method described (SNR = 140.06).

5. The balloon flight

The TIMAX experiment was launched from Birigüi (state of São Paulo, latitude = 21°16'53" S and longitude = 50°19'35" W) in a Winzen stratospheric balloon of 186,000 m^3, on June 8th, 1993, 21:27 UT, by the Balloon Launching Center of INPE. The balloon reached float altitude (42.4 km, 2.1 g cm^{-2}) at $\sim$ 24:00 UT, and remained at this altitude for $\sim$ 8 hours. These were excellent conditions for a balloon flight and astronomical hard X-ray observations. Figure 8 shows the variation of the atmospheric pressure since launch as measured by a pressure sensor installed in the gondola. The accuracy of the sensor is (at float altitude) of the order of 0.01 mbar.

In Figure 9 the temperature variations as function of time are presented as measured by 4 sensors located in different points of the gondola to monitor relevant temperature variations. As can be seen from the Figure, the external temperature at float altitude remained, in average, on the order of -30°C. The precision of the temperature sensor in float altitude is of the order of 1°. This temperature was completely unexpected, since the typical average temperature for 40 km altitude and at 23° S latitude is[27] - 13°C. Due to these anomalous temperatures, even though we have used standard high-density styrofoam thermal insulation (which keeps, on average, the internal temperature 10° C above the external temperature, see Figure 9), the internal temperature (at float altitude) experimented variations from -8° C to–24Á C and this caused the batteries, the power supplies of all detector electronics, to fail $\sim$ 25 minutes after the float altitude has been reached. The housekeeping batteries were different and supported the temperature variations, so we were able to record several on-board parameters (including temperature). Post-flight tests of the detectors batteries in a thermal chamber showed that the batteries begin to fail (that means, the internal chemical reaction stop) at ~ -12°AC, which explain why they did not function where, properly during the flight.

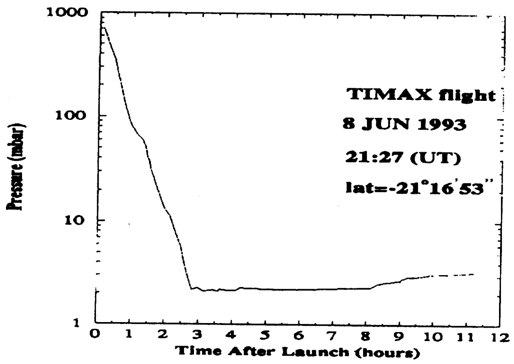

Figure 8: Atmospheric pressure as function of time measured by the TIMAX experiment.

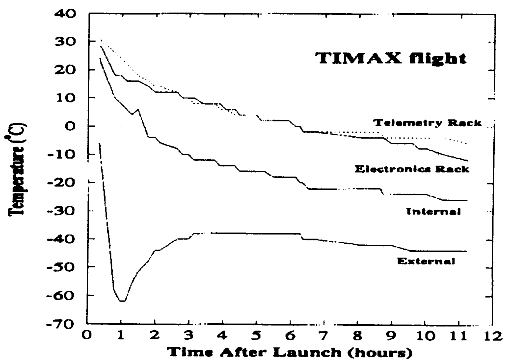

Figure 9: Temperature variations during the flight of the TIMAX experiment, as seen by 4 different sensors.

But we were able to measure the instrumental hard X-ray background spectrum in the float altitude. So we were enabled to calculate the *measured* sensitivity of the telescope. The total counting rate of the background was ~ 40 counts s^{-1} which is in good agreement with the pre-flight estimated[23] count rate of 42 counts s^{-1}. The sensitivity of a X-ray (or γ-ray) telescope is calculated using the expression[28]

$$F = \frac{k}{2A_{ef}\Delta E}\sqrt{\frac{8R_b}{t}}\ , \qquad (4)$$

where

k = number of statistical deviations (number of σ),
A_{ef} = effective area of detector (in cm^2),
ΔE = energy range (in kev),
R_b = background rate (counts s^{-1}),
t = integration time (s).

Figure 10 shows the sensivity of the experiment as a function of energy for several energy bands, and the hard X-ray spectra of some sources: three in the Galactic Center (1E 1740.7-2942, GRS 1758-258 and GX 1+4) and two of the strongest sources in the sky, Crab (nebula and pulsar) and Cyg X-1 (black-hole candidate). As we can see from this Figure, the sensitivity of experiment is such that the scientific objectives of the project can be achieved in a regular balloon flight.

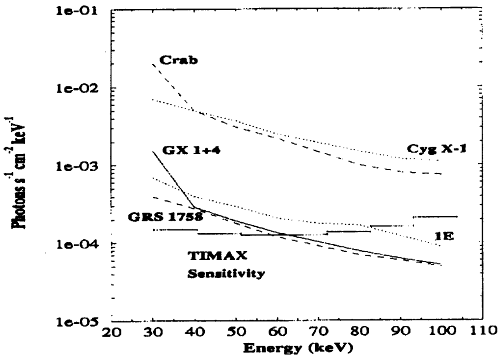

Figure 10: 3σ sensitivity of the TIMAX experiment for an atmospheric depth of 2.1 g cm^{-2} and an integration time of 8 hours. Also shown are the spectra of several X-ray sources: 1E1740.7-2942 ("1E") and GRS 1750-258[29], GX 1+4 at "on" state[30], Crab and Cyg X-1[28].

6. Conclusion

The balloon-borne hard X-ray imaging experiment TIMAX was built, calibrated and flown for the first time in the Southern Hemisphere. Laboratory calibration images have shown that the subtractive mask-antimask technique and the multiplicative correction method are efficient to recover image signal-to-noise ratio lost due to systematic noise in the instrument background and differences in sensitivity across the detector plane. The extrapolation of this method to real astrophysical images is straightforward. The hard X-Ray background measured in the first balloon flight of the experiment enabled us to calculate the sensibility of the experiment, showing that the scientific objectives of the experiment are feasible. This experiment is a prototype of a much larger experiment (called MASCO) currently being built in our laboratory[31].

Acknowledgements

We are very grateful to INPE's balloon group (SLB-INPE) for a perfect balloon flight and all support and friendship during the first TIMAX balloon canlpaign.

Flavio D'Amico gratefully acknowledges CAPES for financial support.

References

1. R. Giacconi, et al., The Astrophysical Journal, **230**, 540 (1979).
2. B. G. Taylor, et al., Space Science Revietos, **30**, 479 (1981).
3. Trümper, J. Advances in Space Research, **2**, 241 (1983).
4. H. Inoue, Experimental Astronomy, **4**, 1 (1993).
5. R. H. Dicke, The Astrophysical Journal Letters, **158**, L101 (1968).
6. E. E. Fenimore, T. M. Canon, Applied Optics, **17**(3), 337 (1978).
7. E. Caroli, et al., Space Science Reviews, **45**, 349 (1987).
8. A. P. Wilmore, et al., Nuclear Instruments and Methods in Physics Research, **221**(1), 284 (1984).
9. W. E. Althouse, et al., Proceedings of the 19th International Cosmic Ray Conference (La Jolla), **3**, 29 (1985).
10. R. A . Sunyaev, et al., Advances in Space Research, **10**(2), 41 (1990).
11. R A. Sunyaev, et al., Advances in Space Research, **10**(2), 233 (1990).
12. J. P. Roques, et al., Advances in Space Research, **10**(2), 223 (1990).
13. W. R. Cook, et al., The Astrophysical Journal Letters, **334**, L87 (1988).
14. P. Hertz, J. Grindlay, The Astrophysical Journal, **278**, 137 (1984).
15. R. Sunyaev, et al., The Astrophysical Journal Letters, **383**, L49, (1991).
16. G. R. Riegler, et al., The Astrophysical Journal Letters, **248**, L13, (1981).
17. R. Sunyaev, et al., The Astrophysical Journal Letters, **389**, L75 (1992).
18. M. Gilfanov, et al., IAU Circular 5474, 1992.
19. R. Sunyaev, et al., Astronomy and Astrophysics, **247**, L29 (1991).
20. 20. G. K. Skinner, et al., Nature, **530**, 544 (1987).
21. U. B. Jayanthi, F. Jablonski, J. Braga, Astrophysics and Space Science, **138**, 183 (1987).
22. 22. M. H. Finger, et al., IAU Circular 5859, 1993.
23. J. Braga, et al., Experimental Astronomy, **2**, 101 (1991).
24. J. Braga, F. D'Amico, T. Villela, Experimental Astronomy, **5**, 269 (1994).
25. M. L. McConnel, et al., The Astrophysical Journal, **321**, 543 (1987).
26. E. E. Fenimore, Applied Optics, **17**, 3562 (1978).
27. J. R. Holton, *The Dynamic Meteorology of the Stratosphere and Mesosphere*, Lancaster Press, 1975.
28. J. Braga., Ph.D. Thesis, Universidade de São Paulo, Brazil, 1990.
29. R. Sunyaev, et al., Astronomy and Astrophysics, **247**, L29 (1991).
30. S. W. B. Dieters, et a.l., Advances in Space Research, **11**(8), 35 (1991).
31. T. Villela, et al., Astrophysics and Space Science, **214**, 161 (1994).